



Article

A Hierarchical Coordinated Control Strategy for Power Quality Improvement in Energy Router Integrated Active Distribution Networks

Xianyang Cui ^{1,2}, Yulong Liu ^{1,2} , Ding Yuan ^{1,2}, Tao Jin ^{1,2,*} and Mohamed A. Mohamed ^{3,*} ¹ College of Electrical Engineering and Automation, Fuzhou University, Fuzhou 350108, China² Fujian Province University Engineering Research Center of Smart Distribution Grid Equipment, Fuzhou 350108, China³ Electrical Engineering Department, Faculty of Engineering, Minia University, Minia 61519, Egypt

* Correspondence: jintly@fzu.edu.cn (T.J.); dr.mohamed.abdelaziz@mu.edu.eg (M.A.M.)

Abstract: The energy router (ER) is a current power electronic device which can integrate distributed energy, provide power for different types of loads, and simultaneously realize the free flow of energy. In traditional active distribution networks, power quality is affected due to the access of photovoltaics (PV) and various loads. Hence, this problem can be improved by accessing the ER. This paper shows the power quality improvement of the grid when the ER is used to integrate PV, energy storage, and AC/DC loads. At the same time, an energy coordination strategy for ER is proposed. The IEEE 13 node model is developed to analyze power quality fluctuations when distributed energy and AC/DC loads are directly connected to the grid. For the power quality analysis, five indicators were selected and the hierarchical analysis method was used to obtain the indicators of power quality. After the use of ER under the coordinated control of ER, the energy is distributed twice and the power quality of the grid improves. The feasibility of ER topology and the control strategy have been verified through an established active distribution networks model with ER. It is verified that when the ER is connected to active distribution networks, the power quality improves accordingly, and it can effectively deal with the characteristics of distributed energy fluctuations and improve the flexibility of the power grid.

Keywords: active distribution network; energy router; energy storage systems; power quality; analytic hierarchy



Citation: Cui, X.; Liu, Y.; Yuan, D.; Jin, T.; Mohamed, M.A. A Hierarchical Coordinated Control Strategy for Power Quality Improvement in Energy Router Integrated Active Distribution Networks. *Sustainability* **2023**, *15*, 2655. <https://doi.org/10.3390/su15032655>

Academic Editors: Hassan M. Hussein Farh, Saad Mekhilef, Ahmed Fathy and Abdullrahman Abdullah Al-Shamma'a

Received: 22 December 2022

Revised: 26 January 2023

Accepted: 28 January 2023

Published: 1 February 2023



Copyright: © 2023 by the authors. Licensee MDPI, Basel, Switzerland. This article is an open access article distributed under the terms and conditions of the Creative Commons Attribution (CC BY) license (<https://creativecommons.org/licenses/by/4.0/>).

1. Introduction

Due to energy scarcity and increasing environmental pollution problems, distributed energy sources have gradually emerged. In this context, traditional centralized systems have gradually transitioned to energy internet (EI) systems, which include distributed renewable energy sources (e.g., photovoltaics) and distributed energy storage devices (e.g., batteries) [1]. The generation from distributed energy sources is commonly unpredictable and its capacity depends on weather conditions [2]. The concept of EI, which allows users to interact with each other to optimize resource allocation, has been proposed because of the high cost of balancing supply and demand through large-scale transmission networks [3,4]. When various distributed energy sources are connected to the grid, they can have negative impacts on the distribution network [5,6], such as increased harmonics, lower power factor, voltage flicker, and voltage transients. The equipment to realize power conversion and power transmission in the traditional distribution network is the power transformer. However, with the development of EI and the diversification of power supply forms, the traditional power transformer can no longer meet the requirements of the future power market, let alone optimize the power quality of the distribution network [7,8]. The use of an energy router (ER) can improve power quality and reduce the harm caused by

distributed energy grid connection. In the context of EI, the widespread use of ER is an inevitable requirement.

Many approaches have been proposed in the literature to improve power quality. For example, the voltage can be increased by compensating the reactive power through shunt capacitors. However, this approach is inflexible and occupies a great deal of space [9]. For power electronic solutions, power quality improvement can be achieved by a distribution static compensator (DSTATCOM) [10], dynamic voltage restorer (DVR) [11], and unified power quality conditioner (UPQC) [12]. A comprehensive description of the various techniques for power quality improvement is provided in [13]. In fact, no matter how the power quality is compensated, it is compensated after the occurrence of the disturbance. The use of ER, which is completely different, reduces the generation of disturbance at the root. When the ER is in some specific operating modes, the effect of distributed energy sources and loads on the distribution grid can be completely eliminated. At present, the research on ER is divided into two levels: the study of ER monolithic structure, control strategy, and application [14], and the study of ER in distribution networks for energy allocation and trend analysis [15]. When connected to ER, the improvement in power quality is noticeable; however, few researchers have investigated this feature.

In terms of the structure and control strategy of ER, Zhen Li et al. proposed an AC/DC hybrid ER coordination control strategy based on energy storage and voltage stabilization, which uses multiple sets of converters to provide rich AC/DC ports [16]. The authors in [17] proposed an energy management strategy based on Lyapunov optimization for optimal control of energy distribution management. Researching from the combination of ER and grid, literature [18] proposes a two-level modular ER structure that can be applied to DC microgrid clusters to achieve a flexible interconnection of microgrids. The implementation of ER is varied and contains different energy. Jordehi et al. [19] combined wind turbines, batteries, and charging stations to establish a reasonable microgrid model. Based on this model, they focused on the impact of flexible resources such as the start and stop of wind turbines, and carried out power market scheduling. In [20], M. Nasir established a new Energy Hub (EH), which also incorporates biomass energy into the energy system to further reduce operating costs. A. Ahmarinejad [21] proposed a long-term perspective, considering the loss of the system. They used the fuzzy maximum value method to model, optimizing the three goals of total cost, emission, and hub losses. This greatly reduced consumption and provided guidance and advice on the operation of carrier energy systems.

Regarding the functionality of ER, the port design and control strategy design are required. Eventually, in combination with distributed energy, a new model of active distribution networks incorporating ER is developed. Compared with the traditional structure, the power quality of the active distribution networks can be effectively improved.

There are various dimensions and metrics for evaluating the power quality of active distribution networks. Regarding the selection and design of indicators, Ref. [22] proposed a regional grid power quality method considering the characteristics. Ref. [23] relies on the establishment of an active distribution network system for PV, wind power, and loads, and establishes an effective power quality classification through the division of different operating modes. Ghada S. Elbasuony et al. proposed a hierarchical analysis method [24], and through the establishment of weight coefficients, the indicators of the hybrid optical storage system offer a comprehensive evaluation of power quality. Yanchun Xu et al. proposed a distributed networks power quality detection method based on variational mode decomposition (VMD) and detrended fluctuation analysis (DFA) cooperation [25]. This paper starts from the classification of power quality disturbances and addresses the power quality evaluation system. However, there are numerous classification indexes, and the classification accuracy is reduced. Ref. [26] proposes a control scheme adapted to large power systems with input and output constraints, modeled using fuzzy systems, which verifies the feasibility of the control strategy under load fluctuations. S. A. Mansouri [27] considered the information interconnection and sharing of decentralized microgrid struc-

tures to design hierarchical models that reduce their complexity, improve the resilience index, and provide a solution for the complex system of the dispatch configuration.

Under the existing research system, for the active distribution networks with integrated source-grid-load-storage, energy dispatching generally must be performed according to the current power flow. Alternatively, extra compensation devices can be added, but none of these methods can eliminate the impact from load fluctuation or energy fluctuation at the root. The difference is that ER takes an entirely different perspective by accommodating source storage and load into a different system. ER carries out energy transfer through the internal DC bus and eventually connects to the distribution grid through the grid-connected port. Under the improved active distribution networks constructed through the ER, the fluctuation of load and new energy can be entirely isolated from the distribution network under some working conditions. Finally, the power quality of the distribution networks can eventually improve.

In response to the development status of active distribution networks with integrated source-network storage and load, a five-port ER topology is proposed. The five ports are respectively connected to the grid, energy storage, AC load, DC load, and PV. At the same time, the corresponding port coordination strategy is designed. In addition, an analytical hierarchy process is used to analyze power quality. It is verified that under the application of ER, the power quality has improved.

The main innovation points of this paper are summarized as follows:

1. A five-port ER with PV, energy storage, grid-connected, AC load, and DC load ports is set up for the current development of active distribution networks. Based on the topology of the ER and the energy flow, a hierarchical control strategy is designed to conform to this structure and achieve a coordinated operation of the five ports and free energy flow.
2. The ER system is integrated into the active distribution network to build an active distribution network system with energy routers. All ports are connected through the DC busbar. At the same time, a port control strategy matching the structure and energy scheduling strategy are designed. The power quality is analyzed using hierarchical analysis, and the feasibility of the ER system and the power quality improvement are verified.

The rest of this paper is organized as follows: Section 2 introduces the system establishment and control realization. Section 3 presents the establishment of the power quality evaluation system. Section 4 shows the simulation analysis and results. Finally, the conclusion of this paper is introduced in Section 5.

2. System Establishment and Control Realization

2.1. Power System Structure Establishment

Figure 1 shows the traditional distribution network model and the distribution network model including ER, respectively. The IEEE13 node model is used, which includes PV and AC/DC loads [28,29]. Unlike the traditional distribution network model, a new active distribution networks model containing ER is proposed. In the new system, the PV, AC loads, and DC loads are connected to the distribution network through ER. Due to the use of ER, the traditional power system structure has changed and the power quality will improve.

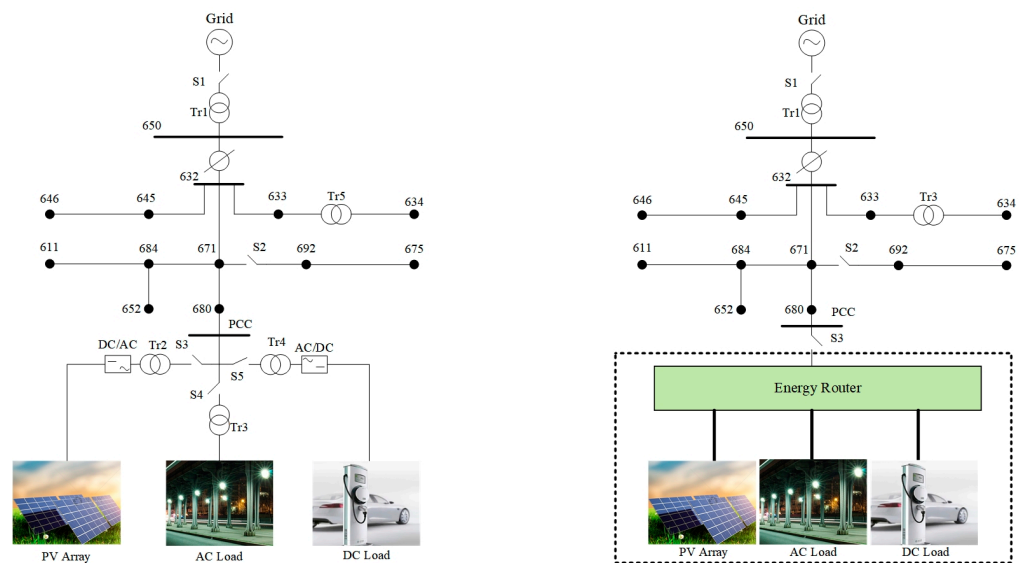


Figure 1. Traditional distribution network model and distribution network model with ER.

As shown in Figure 1, there are two different systems. The following sections start from the structure of ER to analyze the changes to the system.

2.2. ER topology Establishment

Aiming at the PV characteristics and the use of AC/DC load, a five-port ER is proposed in this paper. The architecture of a five-port ER is shown in Figure 2. The five ports are a grid-connected port, PV port, energy storage port, DC load port, and AC load port. The grid-connected port is connected to the distribution network. All ports of the ER converge into a DC common bus (CB). All ports of the ER converge into a DC common bus. All devices interact with each other via DC buses.

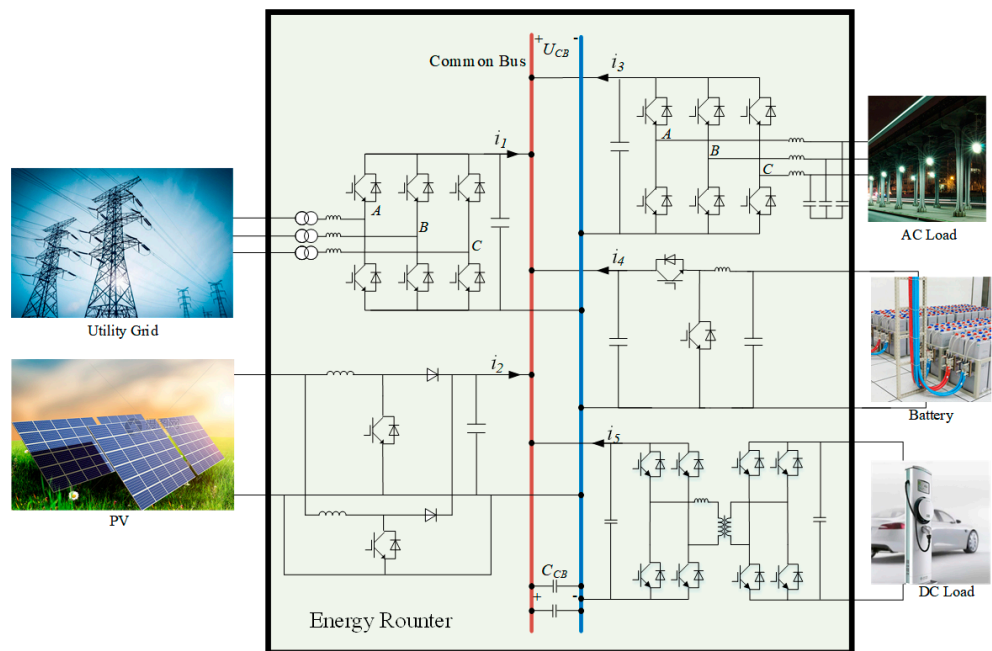


Figure 2. Structure of five-port ER system.

Combining the characteristics of the distribution network and the actual load conditions, the ER has five external ports, which are connected to the utility grid, PV, AC load, energy storage, and DC load.

The first is the grid-connected port, which adopts the structure of a three-phase inverter. This is the core port in the ER system that enables a bidirectional flow of energy. The second port is the PV port. The function of the PV port is to incorporate solar energy into the ER system, and the criterion of its work is the full utilization of light energy without considering additional factors such as energy flow and system stability. The design and control of the PV port starts from the efficient acquisition of energy without involving other factors. Considering the characteristics of a low PV voltage level, multiple parallel PV cells, and a high DC bus voltage level, a boost converter is used as the port. Considering the expandability and the current stress of the IGBT, an interleaved parallel boost circuit is adopted. When the power is the same, interleaved parallel booster structure switch current stress is smaller compared with the ordinary booster circuit, and current ripple is also smaller. This configuration has advantages in terms of the stability of the common bus voltage and control of the current.

The next is the energy storage port. This port connects the energy storage battery to the DC bus through a bidirectional buck-boost circuit. It plays the role of energy buffer. This port needs to realize the bidirectional flow of energy, and it also requires rapid control to quickly sense the fluctuation of the common bus voltage, so adjustments are made in the control. The bidirectional buck-boost structure is chosen for the structure, and the model predictive control is used for the control.

Finally, the design of the AC and DC load ports also plays an important role in ER. Considering the controllability of the system and the difficulty of the overall control, these two ports do not participate in the control of the voltage stability of the common bus, but only serve as functional ports for the load. Both ports use the conventional control strategy matched with the structure to ensure output stability and achieve basic external functions.

The energy interactions of all ports need to pass through the DC common bus. The stability of DC common buses is fundamental to the stable operation of the ER system. The energy interaction per unit time has the following formula:

$$U_{CB}i_1\Delta t + U_{CB}i_2\Delta t + U_{CB}i_3\Delta t + U_{CB}i_3\Delta t + U_{CB}i_4\Delta t + U_{CB}i_5\Delta t + \frac{1}{2}C_{CB}U_{CB}^2\Delta t = 0 \quad (1)$$

$$\sum_{j=1}^5 P_j\Delta t + \frac{1}{2}C_{CB}U_{CB}^2\Delta t = 0 \quad (2)$$

The control of energy flow is realized through Equation (2), when the system loss is not considered and the common bus voltage is stable, which means that the energy flow control is stable.

For the ER, the focus is on the flow of energy. Since the analysis is the impact on the power grid, the grid-connected port is the most important port that needs to be considered. Figure 3 shows the power electronic structure of the net-connected port of the ER.

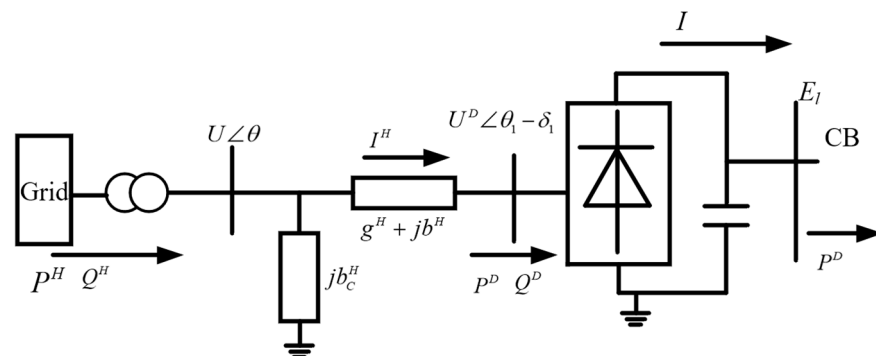


Figure 3. Power electronic structure of the net-connected port of the ER.

The grid-connected port is connected to the grid at one end and to the common bus CB at the other end, as shown in Figure 3, while the other ports are also connected by the CB. For the grid-connected ports, there are the following energy relations. First, the power loss of the port can be equivalently represented by the derivative $g^H + jb^H$. The reactive power loss of the joint can be equated by jb_C^H .

The energy obtained from the grid-connected ports is absorbed by the rectifier in the reactive part after the conductance and the electronation, and the active part of energy is then transferred to the DC bus to supply the other ports and participate in the overall energy balance. The overall energy balance equations are expressed as follows:

$$P^H = g^H U^2 - (g^H \cos \delta_1 + b^H \sin \delta_1) U U^D \quad (3)$$

$$Q^H = -(b_C^H + b^H) U^2 + (b^H \cos \delta_1 - g^H \sin \delta_1) U U^D \quad (4)$$

Assuming there is no energy loss in the rectifier section, the energy interacting with the common bus is

$$P^D = E_l I = -g^H (U^D)^2 + (g^H \cos \delta_1 - b^H \sin \delta_1) U U^D \quad (5)$$

$$E_l = w U^D \quad (6)$$

where w is the converter equivalent control coefficient, which is related to the converter topology and the control strategy. Our task is to control the converter to achieve energy interaction.

Figure 4 shows the energy flow and the information flow between an ER Centralized Controller (ERCC), the five ports, and the common bus.

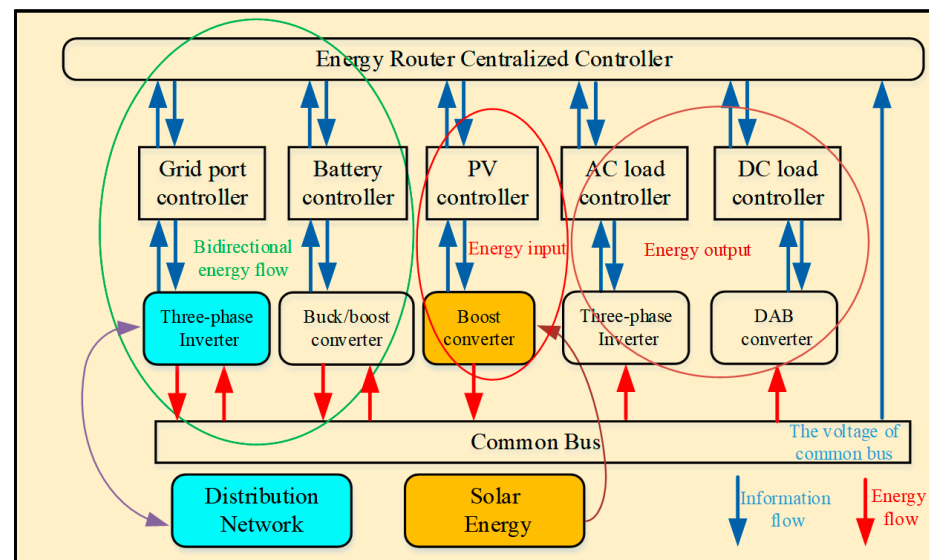


Figure 4. The information and energy flow of ER.

Figure 4 shows that the control of ER is divided into two levels: module-level control and system-level control. Figure 4 demonstrates that the energy storage and grid-connected ports are bidirectional ports, which play a role in coordinating energy and stabilizing the common bus voltage, and have a higher position in the overall control. The AC load port, DC load port, and PV port are directly connected to the common bus. These three ports are only responsible for a one-way energy transmission. For the control of these ports, only the external functions need to be realized. The influence on the common bus of the ER is stabilized by the bus capacitor and balanced by the bidirectional port. Thus, the control of the grid connection and the energy storage port is based on the stability of the bus voltage.

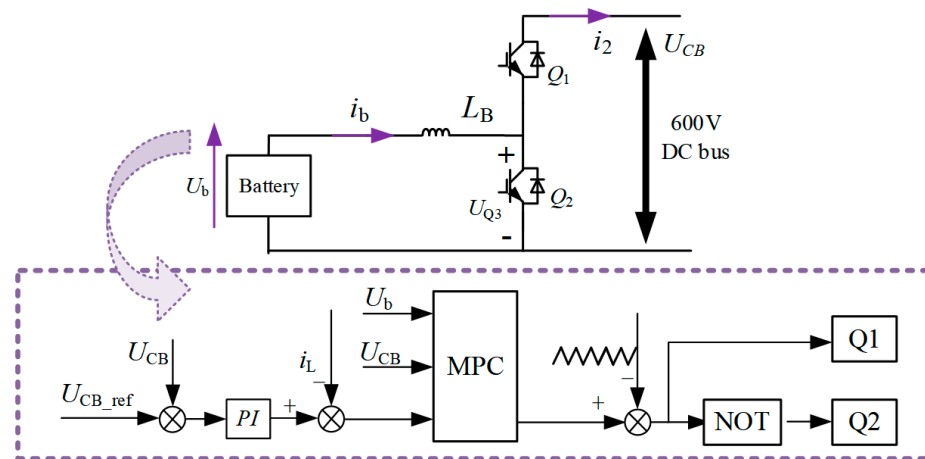


Figure 6. Energy storage port control strategy diagram.

From the structure diagram of energy storage port

$$U_Q = L_B \frac{di_b}{dt} + U_b \quad (8)$$

We can discrete Formula (4) and then we can get

$$i_L(k+1) = (U_Q - U_b) \frac{T_s}{L_B} + i_L(k) \quad (9)$$

The inductance current at k time can be obtained by sampling, and the inductance current at $k+1$ time can be predicted. The battery terminal voltage is lower than the common bus voltage, and the converter operates in Buck mode, with $U_Q = DU_{CB}$. After substituting Formula (9):

$$i_L(k+1) = (DU_{CB} - U_B) \frac{T_s}{L_B} + i_L(k) \quad (10)$$

Considering that the digital control system has a beat delay, it is necessary to use the sampling value at time k to predict the inductance current value at time $k+1$, and use this value to predict the reference current value at the next beat. The delay expression of one beat is as follows:

$$i_L(k+1) = (D_{old}U_{CB} - U_B) \frac{T_s}{L} + i_L(k) \quad (11)$$

where D_{old} is the duty cycle of the previous time. Generally, the sampling time is short, so the DC bus voltage U_{CB} and the battery voltage U_B remain unchanged at k and $k+1$. Therefore, the duty cycle at the next time can be calculated by the following expression:

$$D = \frac{(i_{L_ref} - i_L(k+1))L}{T_s U_{CB}} + \frac{U_B}{U_{CB}} \quad (12)$$

Finally, the control block diagram of the energy storage converter in Figure 6 is obtained. First, the DC bus side voltage U_{CB} and the given reference voltage U_{CB_ref} are sent to the proportional integral PI for comparison. At this time, a reference current is output to compare with the actual inductance current, and is sent to the model predictive controller to generate the duty cycle. The output is compared with the carrier to generate the control signal of the switch. When the bus voltage fluctuates, the model predictive control strategy can be used to adjust.

In the ER system, the grid-connected port and energy storage port are bidirectional ports, and the coordination control of the ER comes from the control of these two ports. When an energy imbalance occurs, the energy storage port and the grid-connected port are

fed, respectively, according to their respective states to replenish the unbalanced energy. According to Formula (2), the voltage stability of a common bus is equal to the balance of the overall energy. Thus, port control starts from the voltage stab.

A set of nine working models have been established of ER operation by dividing the working modes of the ports and the current state of energy storage. This working mode corresponds to the work of the energy storage port as well as the grid-connected port above, and since these two ports are bidirectional ports, we define the direction of energy flow, with energy flowing out from the common bus as + and energy flowing into the common bus as −.

As can be seen in Table 1, the operating models of the ER are divided into nine groups, starting with BEH, which is the ideal state of three groups, in which the energy router is considered an island, the PV supplies energy directly to the load, and there are no other energy interactions. Models A and G indicate that the PV is sufficient, the battery port is working, and the ER stores energy. FI indicates that the storage is sufficient and the battery provides energy to the load for consumption. Finally, Models C and D indicate that the energy router has no way to handle the energy gap by itself and needs the participation of the grid-connected port, which will have an impact on the power quality.

Table 1. Working mode of ER.

Model	Energy Value Comparison	Battery SOC	Energy Storage Port	Grid Connected Port
Model A	$P_{load} < P_{PV}$	SOC < 10%	+	0
Model B	$P_{load} = P_{PV}$	SOC < 10%	0	0
Model C	$P_{load} > P_{PV}$	SOC < 10%	0	+
Model D	$P_{load} < P_{PV}$	SOC > 90%	0	-
Model E	$P_{load} = P_{PV}$	SOC > 90%	0	0
Model F	$P_{load} > P_{PV}$	SOC > 90%	-	0
Model G	$P_{load} < P_{PV}$	10% < SOC < 90%	+	0
Model H	$P_{load} = P_{PV}$	10% < SOC < 90%	0	0
Model I	$P_{load} > P_{PV}$	10% < SOC < 90%	-	0

3. Establishment of Power Quality Evaluation System

3.1. Selection of Power Quality Evaluation Indicators

The harmonic distortion is caused by various types of harmonic generation equipment. In most cases, when the distributed generation unit is connected to the nonlinear load, the harmonic distortion of the distribution system will increase. According to IEEE 519, THD_v and THD_i are taken as PQI indicators of harmonic distortion, and the harmonic times at point of common coupling (PCC) are generally calculated to 40, as shown in Formulas (13) and (14).

$$THD_v = \sqrt{\sum_{h>1}^{h=40} |V_h|^2} / V_1 \quad (13)$$

$$THD_i = \sqrt{\sum_{h>1}^{h=40} |I_h|^2} / I_1 \quad (14)$$

In Formulas (9) and (10), V_h and I_h are, respectively, the effective values of the hth-degree harmonic current and voltage measured at PCC. V_1 and I_1 are the effective values of their fundamental waves. According to IEEE 519, THD_v and THD_i values do not exceed 5% for the system.

IEEE Std. 1159 defines voltage sag and rise as the phenomenon that the effective value of voltage shifts within 0.5 cycle to 1 min. Based on this, this paper calculates the

voltage offset score (ADS) from the effective value of three-phase (V_a, V_b, V_c) voltage. The expression is given in Equation (15).

$$ADS = \frac{|1 - V_a| + |1 - V_b| + |1 - V_c|}{3} \times 100 \quad (15)$$

The standard definition of a frequency shift is an increase or decrease in the power system's power frequency, which can last from a few cycles to several hours. According to EN 50160, within 95% of a cycle, the frequency range fluctuation shall be within a % of the rated frequency (50 or 60 Hz). During an entire cycle, the frequency range fluctuations shall be within $-6\%/ -4\%$ of the rated frequency. The definition of frequency offset ratio (FDR) is shown in Equation (16).

$$FDR = \frac{|f_m - f_1|}{f_1} \times 100 \quad (16)$$

where f_m is the measured voltage fundamental frequency, which changes over time, and f_1 is the rated frequency of the system.

Power factor (PF) is the ratio of active power to apparent power. Low PF values are derived from inductive loads such as induction motors, transformers, etc. The real power factor measured in PCC shall be kept within the acceptable range ($>90\%$) to improve the energy transfer efficiency of the system, as shown in Equation (17).

$$PF = \left(P_1 + \sum_{h>1}^{40} P_h \right) / \left(S_1 + \sum_{h>1}^{40} S_h \right) \quad (17)$$

where P_1 and S_1 are the active power and apparent power of fundamental wave signal transmission at the monitoring point, respectively. P_h and S_h are the active and reactive power of the h th-degree harmonic.

3.2. Power System Quality Evaluation Index Based on Analytic Hierarchy Process

The analytic hierarchy process (AHP) is a systematic and hierarchical decision-making analysis method that combines quantitative and qualitative analysis. It forms a judgment matrix based on the comparison between two different attributes and uses the largest eigenvalue of the judgment matrix to compute the weight of each attribute. The steps of AHP are as follows:

- (1) Build a hierarchical model and a judgment matrix.
- (2) Calculate the maximum eigenvalue of the judgment matrix λ_{\max} and the corresponding eigenvector. The element of the feature vector corresponds to the weight of each attribute.
- (3) Calculate the consistency index (CI) and consistency ratio (CR), and check whether the results meet, as shown in Equation (18).

$$\begin{cases} CI = (\lambda_{\max} - N_f) / (N_f - 1) \\ CR = CI / RI \end{cases} \quad (18)$$

Here, N_f is the dimension of the judgment matrix and RI is the average random consistency index related to the dimension of the judgment matrix. There are five indexes for power quality evaluation in this paper, and the order is five, and RI is taken as 1.26. The basic scale of comparison is 1–9, as shown in Table 2.

Table 2. Scale table of AHP.

Quantization Scale (<i>i</i> Relative to <i>j</i>)	Meaning
1	<i>i</i> is as important as <i>j</i>
3	<i>i</i> is slightly more important than <i>j</i>
5	<i>i</i> is generally more important than <i>j</i>
7	<i>i</i> is significantly more important than <i>j</i>
9	<i>i</i> is extremely important compared with <i>j</i> PCC
2, 4, 6, 8	The median value of the above two adjacent judgments

In the system of this study, five indicators are proposed in this section to evaluate the power quality: THD_v , THD_i , ADS , FDR , and $1/PF$. The inverse of power factor is considered here, so that the smaller the value of all six indicators, the better the power quality and the higher the evaluation.

In different systems, different indicators have different weight coefficients. This study focuses on the power quality at PCC bus. Usually PCC bus is a new energy grid point, so THD_v , and FDR are more important. Based on experience, this paper considers two modes of PCC, sets different weight coefficients, and obtains the power quality evaluation values of PCC, respectively.

The two used settings are as follows: THD_i is assumed to be the most important indicator affecting power quality; it is assumed that ADS is the most important element affecting power quality, and its judgment matrix is shown in Table 3. The evaluation of the comparison matrix is confirmed to be consistent by the calculation of the consistency ratio. Synthesizing the three weight vectors of the three assumptions, the average reliable weight vector of this type of bus is $W_{pcc} = [0.1281, 0.2884, 0.2622, 0.2612, 0.0602]^T$.

Table 3. Judgment matrices and the resultant weight vectors of the two scenarios of PCC bus.

Scenario1	THD_v	THD_i	ADS	PDR	$1/PF$
THD_v	1	1/3	2	1/2	3
THD_i	3	1	4	2	5
ADS	1/2	1/4	1	1/3	2
PDR	2	1/2	3	1	4
$1/PF$	1/3	1/5	1/2	1/4	1
$\lambda_{max} = 5.0681, CI = 0.0255, CR = 0.0170 < 0.1$ (Accept) Weight vector [0.1599, 0.4186, 0.0973, 0.2625, 0.0618]T					
Scenario2	THD_v	THD_i	ADS	PDR	$1/PF$
THD_v	1	1/2	1/4	1/3	2
THD_i	2	1	1/3	1/2	3
ADS	4	3	1	2	6
PDR	3	2	1/2	1	4
$1/PF$	1/2	1/3	1/6	1/4	1
$\lambda_{max} = 5.0490, CI = 0.0123, CR = 0.009 < 0.1$ (Accept) Weight vector [0.0962, 0.1581, 0.4272, 0.2599, 0.0585]T					

The PQI can be calculated on PCC in two cases through the average weight vector, and we can get the final point energy quality evaluation index from Equation (19).

$$PQI = \sum_{p=1}^{N_f} w_p F_p, \sum_{p=1}^{N_f} w_p = 1 \quad (19)$$

In the Formula (19), N_f is the number of selected indicators that affect power quality, and F_p and w_p are the measured values and corresponding weights of indicator p . Therefore, in this paper, the PQI calculation formula can be rewritten as

$$PQI = w_1(THD_v) + w_2(THD_i) + w_3(ADS) + w_4(PDR) + w_5(1/PF) \quad (20)$$

4. Simulation Analysis and Results

The first step is to verify the feasibility of the ER topology and control strategy. The basic parameters of the system are set according to Table 4.

Table 4. System parameters.

Modular	Parameter	Value
Common bus	Common bus voltage	600 V
	Parallel strings	600
PV port	Series-connected modules per string	6
	Voltage at maximum power point	43 V
	Current at maximum power point	8.13 A
	Maximum power	1.25 MW
Battery port	Rated capacity	500 Ah
	Normal voltage	500 V
	Fully charge voltage	581 V
AC load port	Full load power	1 MW
	Rated voltage	AC 380 V
DC load port	Full load power	1 MW
	Rated voltage	DC 200 V
Grid port	Standard voltage(single-phase)	1650 V
	Standard frequency	60 Hz

Based on the parameters listed in the table above, simulations of the energy router were performed to verify the feasibility of the control.

The total simulation time is 2 s. The working state of the system is shown in Figure 7. It consists of four parts and the second graph represents the state of the external environment. At the beginning, the PV and AC ports work.

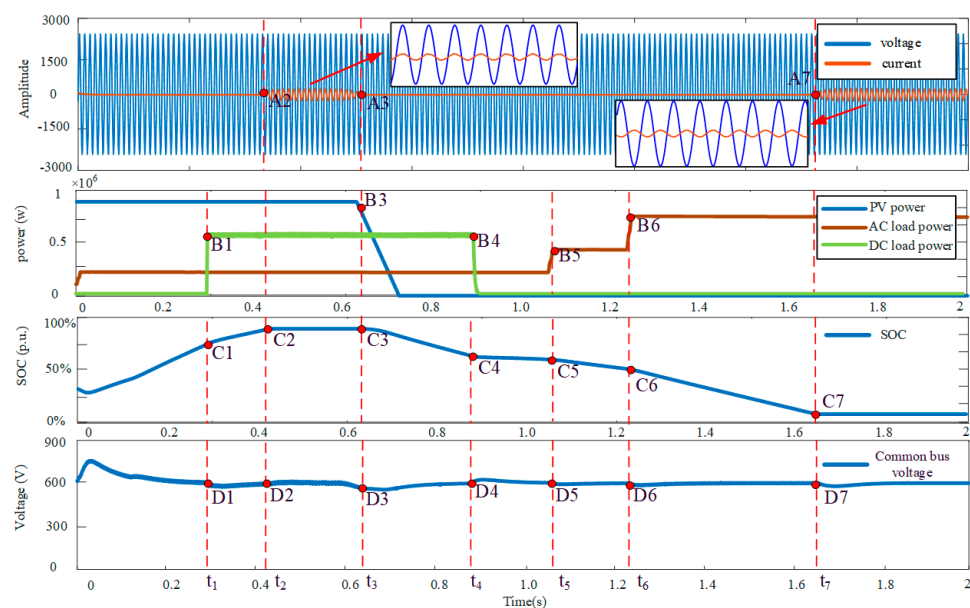


Figure 7. ER port power and internal state diagram.

B1: DC port starts to work.

B3: PV port power gradually decreases to 0.

B4: DC port power decreases to 0.

B5: AC port power increases.

B6: AC port power increases.

The first graph shows the voltage and current at phase A of the grid-connected port, the third graph shows the energy storage SOC, and the fourth graph shows the common bus voltage values. These three graphs reflect the ER's response to changes in the external environment.

$t_0 - t_1$: During this time, the PV power is elevated, the AC load is working, and the energy storage is insufficient. We can see the SOC increase gradually.

$t_1 - t_2$: During this time, the DC port starts working, the PV power is still greater than the load power ($P_{ACload} + P_{DCload}$), the SOC still rises, but the slope of the C1 to C2 segment is lower.

$t_2 - t_3$: During this time, the energy storage is full, C2 to C3 is a straight line and the grid-connected port starts working to transfer the excess energy to the grid side. From A2 to A3, it can be seen that the voltage and current direction are the same, and the power is positive.

$t_3 - t_4$: During this time, the power of the PV port gradually decreases to 0 and the energy storage port supplies energy to the AC and DC ports, at which point the SOC decreases.

$t_4 - t_5$: During this time, DC port power is reduced to 0 and only the AC port consumes energy. Correspondingly, the battery discharges slower and the SOC decreases slower.

$t_5 - t_6$: During this time, the AC port power increases further, the battery discharges faster, and the SOC decreases faster.

$t_6 - t_7$: During this time, the battery is depleted and the grid-connected port reengages, but the energy transfer is in the opposite direction from $t_2 - t_3$.

The fourth graph shows the fluctuation of the common bus voltage, which fluctuates during modal switching, but quickly returns to stability. The ER can work stably under the proposed control strategy and the free flow of energy is successfully achieved.

According to the mode division of ER and the state of lighting and energy storage, two experiments were carried out to verify the correctness of the theory.

Experiment 1 was implemented in this way:

The PV module is added to the IEEE13 node model with ER and the IEEE13 node model without ER, respectively, both using MPPT for maximum power tracking and varying the light intensity to obtain the metrics proposed above.

For conventional systems (the structure on the left of Figure 1), we can obtain the conclusion of Figures 8–11.

The first graph in Figure 8 shows the PCC bus voltage, the second graph represents the PV power fluctuation, and the third graph shows the amplitude-frequency-time contours of the voltage measured at the PCC bus of the distribution system drawn after S-transformation. The vertical axis is the signal frequency, the horizontal axis is time, and the color represents the amplitude magnitude.

The first is the incorporation of PV and the power fluctuation situation, which is an important factor causing the generation of system harmonics.

The system starts with the PV power set to 0.37 MW, and in 0.2 s the PV power starts to rise and eventually reaches 1 MW. Considering the realistic situation, the Rate Limiter module is used in Simulink, so the PV power is slowly increased in 0.1 s. The PV power then drops at 0.5 s and ends up at 0.77 MW.

Fluctuations in the PV power lead to fluctuations in the voltage, but this is not particularly pronounced, as we can see from the amplitude-frequency-time conversion plot. There is a magnitude fluctuation at 0.2–0.3 s and a magnitude fluctuation at 0.5–0.6 s, which corresponds to the shift of PV power. When the PV power does not change, the amplitude-frequency-time conversion fluctuates slightly, but not significantly.

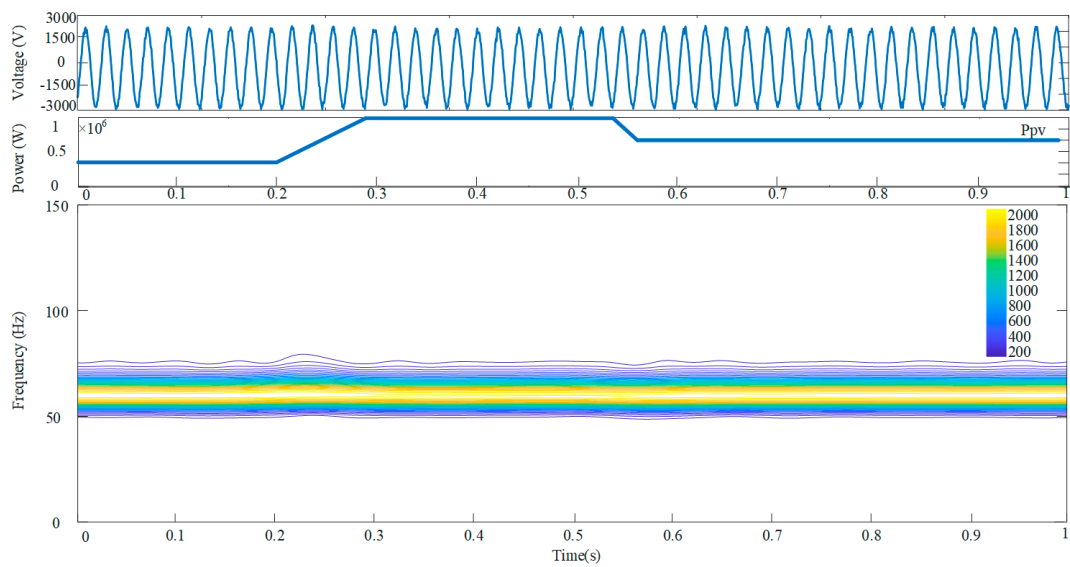


Figure 8. Ex1.PCC voltage, power of PV, amplitude-frequency-time contours-without ER.

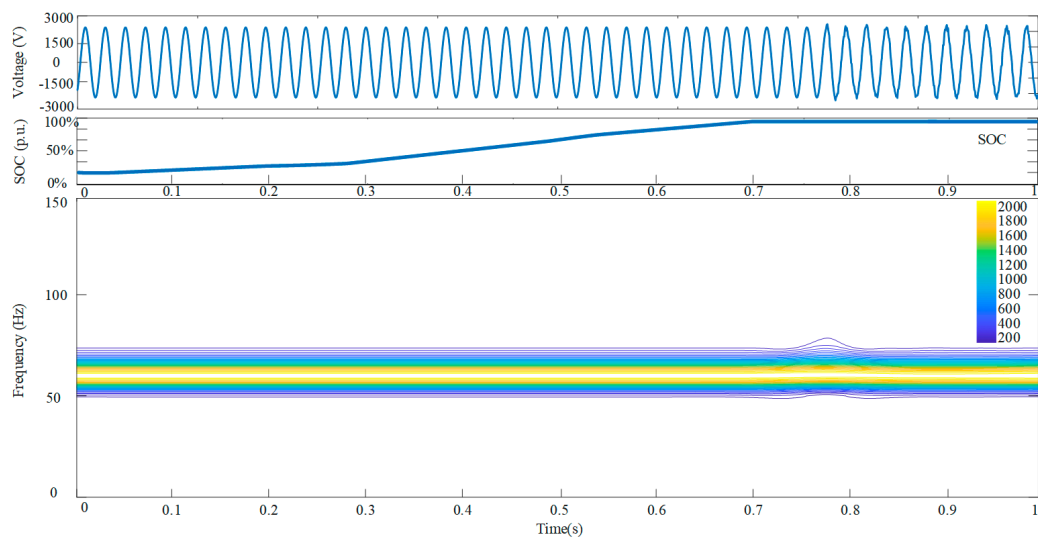


Figure 9. Ex1.PCC voltage, energy storage soc, amplitude-frequency-time contours-with ER.

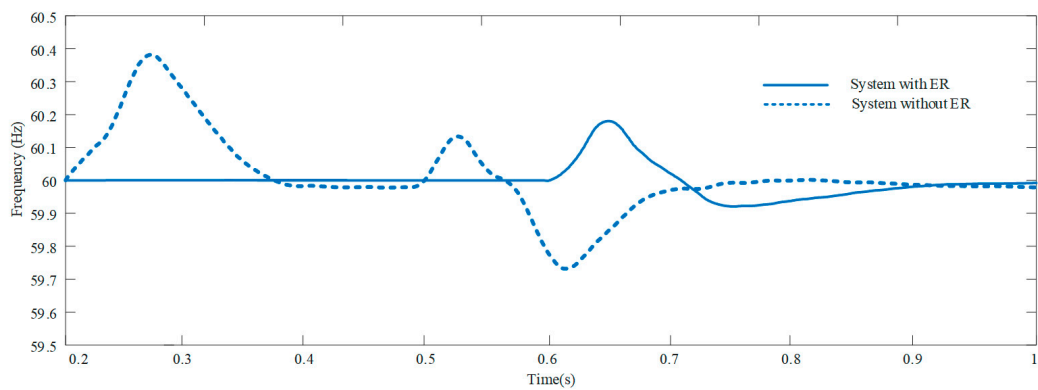


Figure 10. Ex1.FDR—TIME.

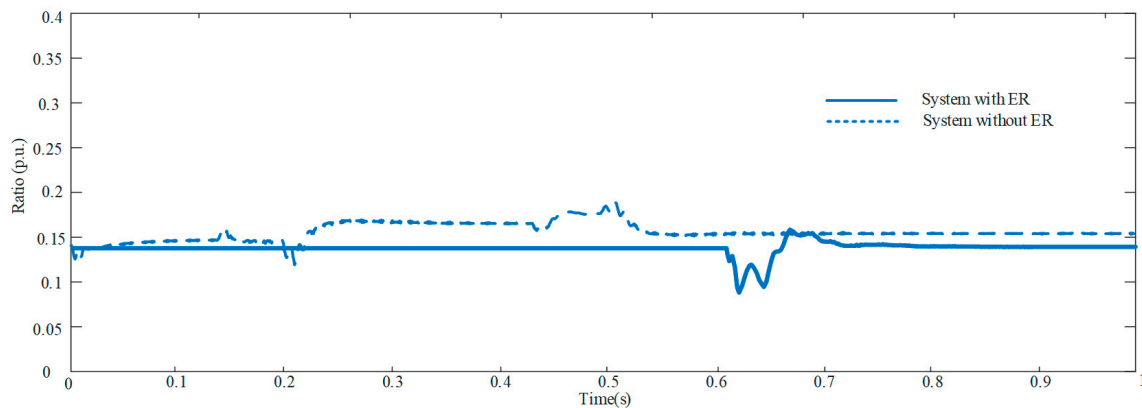


Figure 11. Ex1.ADS—TIME.

For systems with ER (the structure on the right of Figure 1), we can obtain the conclusion of Figures 9–11.

The first graph in Figure 9 shows the PCC bus voltage, the second graph represents the SOC of battery, and the third graph shows the amplitude-frequency-time contours of the voltage measured at the PCC bus.

Due to the access of the ER, the injection of PV energy is buffered; ER first dissipates the energy generated by PV without injecting it directly into the grid. When the battery used for energy storage is full, the energy goes only to the grid side. The SOC reflects the process of gradually filling the energy storage, with the SOC gradually rising before 0.3 s and rising at a faster rate after 0.3 s, corresponding to an increase in the PV energy intensity. At 0.7 s, the SOC reaches the maximum, which means the energy storage is full, and then the charging is stopped and the excess energy is injected into the grid. In the third figure, the difference between the system with ER and the normal system can be seen. Due to the use of ER, the optical conversion is completed without any impact on the back-end grid when the energy storage is used, and after the energy storage is full, control strategies can be used to reduce the impact on the grid ports.

Figures 10 and 11 show the images of *FDR* and *ADS* with time for the system with ER and the system without ER, respectively. Since the *FDR* acquisition uses a phase-locked loop, it takes time for the system to stabilize, so the data are acquired from 0.2 s. In both images, the solid line indicates the system with ER and the dashed line indicates the conventional system (without ER). It is obvious that the conventional system is affected by the external environment, which brings about the deterioration of the steady state, while the system with ER is considered an isolated system in some modes, so it does not have any effect on the nodes.

Experiment 2 was implemented in this way:

In the absence of PV access, the DC load is increased in the form of observing the voltage fluctuations at the nodes while obtaining the relevant parameters. At the very beginning, the load power is 0.35 MW, and at 0.4 s, the load power is increased to 0.5 MW and maintained at 0.5 MW until the end.

As shown in Figure 12, the load power is 0.35 MW before 0.35 s. In the third figure, there is not too high harmonics present in the system, and at 0.35 s the load increases and a voltage transient occurs, accompanied by an increase in harmonics, which eventually stabilizes.

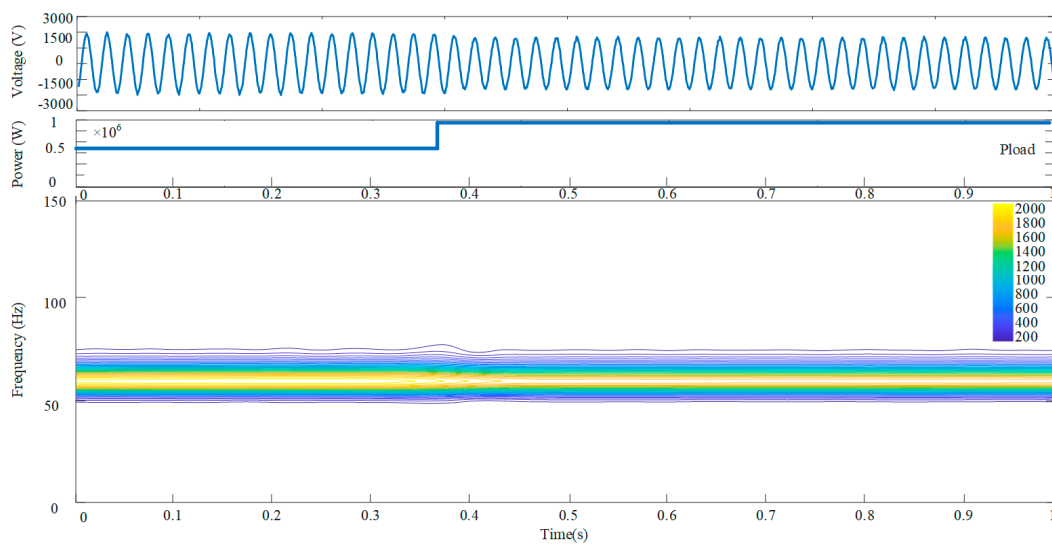


Figure 12. Ex2.PCC voltage, power of load, amplitude-frequency-time contours—without ER.

Figure 13 shows the ER voltage, energy storage SOCs, and amplitude-frequency-time. The external environmental changes are consistent with those in Figure 11. The second figure represents the SOC of the energy storage. At the beginning, the energy storage is sufficient and the ER operates in mode I, which means that all the consumption of the load is provided by the energy storage. We know that when the ER is working in Model I, the grid-connected ports do not work, so the change in external load does not affect the power quality at the PCC bus at all. Therefore, the PCC voltage does not fluctuate at all during the first half of the simulation and the system is extremely stable.

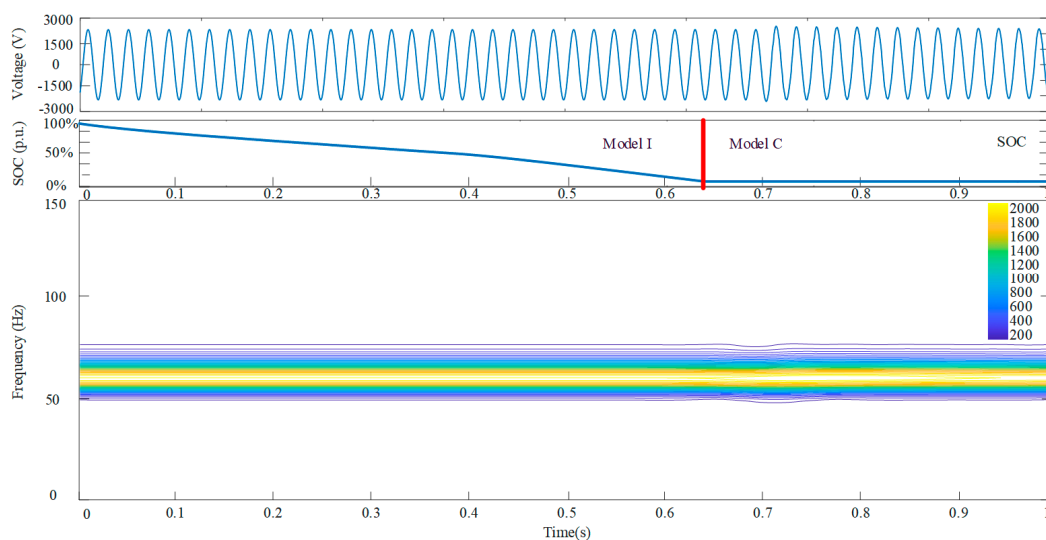


Figure 13. Ex2.PCC voltage, energy storage soc, amplitude-frequency-time contours—with ER.

At about 0.63 s, the energy storage is depleted and no PV energy or other energy is replenished. The system needs to consume energy to supply the load for use, at which point the system enters Model C. Under Model C, the energy storage port of the ER system does not work, and all the energy consumed by the load is supplied by the grid-connected port. The switching of the system modes causes the voltage to fluctuate, but it soon stabilizes.

Figure 14 indicates the FDR at the PCC bus with and without the ER system. For the FDR, the results were not significantly different between the two groups. However, the system using the ER is obviously more stable in the first half.

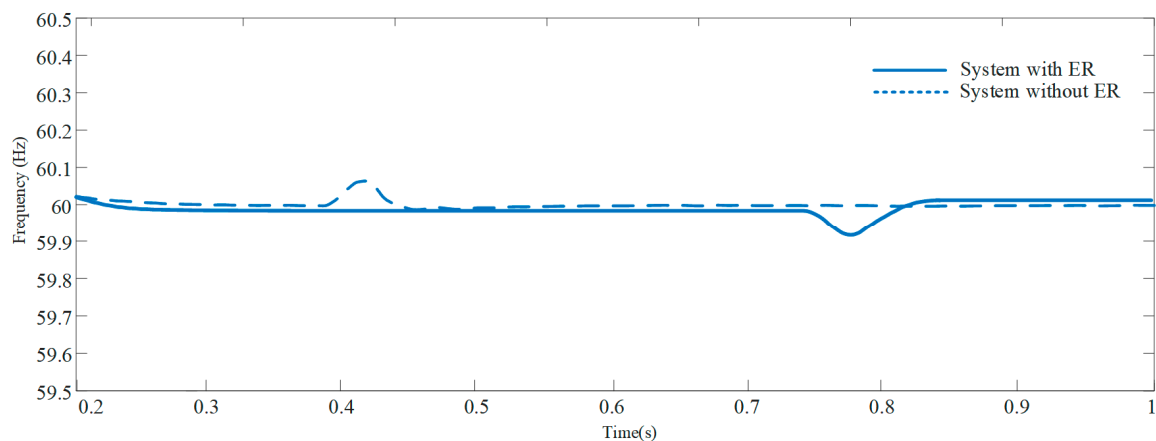


Figure 14. Ex2.FDR—TIME.

All the possible conditions are classified into ten types according to the mode of operation of the ER, and nine simulation experiments are carried out to obtain the PCC bus parameters with and without the ER. Nine typical cases are selected for analysis as follows:

For ordinary systems without ER and without energy storage SOC, the PV and load are connected to the PCC port simultaneously with the same power described below. Table 5 shows the experimental results and power quality parameters.

Table 5. Experimental results and power quality parameters.

	Situation		THD_v	THD_i	ADS	FDR	$1/PF$	PQI
1	ER	EX1-1	0.01	0.01	0.00	0.02	1.40	0.094
	without ER	EX1-2	2.52	0.74	0.69	0.20	1.95	0.823
2	ER	EX2-1	2.04	0.40	0.95	0.10	2.04	0.769
	without ER	EX2-2	3.04	1.20	0.20	1.00	2.10	1.170
3	ER	EX3-1	2.48	0.58	0.01	0.10	1.30	0.583
	without ER	EX3-2	2.65	0.60	1.40	0.50	3.00	1.184
4	ER	EX4-1	0.01	0.01	0.00	0.02	1.40	0.094
	without ER	EX4-2	2.00	0.75	1.44	0.02	1.76	0.961
5	ER	EX5-1	0.01	0.01	0.00	0.02	1.40	0.094
	without ER	EX5-2	2.50	0.60	0.00	0.10	1.40	0.604
6	ER	EX6-1	0.01	0.01	0.00	0.02	1.40	0.094
	without ER	EX6-2	2.53	0.50	2.00	1.00	2.00	1.370

Situation 1: $P_{load} = 0.45$ MW, $P_{PV} = 0.85$ MW, SOC = 5;

Situation 2: $P_{load} = 0.75$ MW, $P_{PV} = 0.4$ MW, SOC = 5;

Situation 3: $P_{load} = 0.55$ MW, $P_{PV} = 1$ MW, SOC = 95;

Situation 4: $P_{load} = 0.75$ MW, $P_{PV} = 0.4$ MW, SOC = 95;

Situation 5: $P_{load} = 0$ MW, $P_{PV} = 0.5$ MW, SOC = 65;

Situation 6: $P_{load} = 0.5$ MW, $P_{PV} = 0$ MW, SOC = 65;

Based on the formula of the hierarchical analysis method proposed above, we can conclude that when the hierarchical analysis method is used, the power quality indicators fluctuate in the above six cases. It is worth noting that the power quality indicators of the system with the presence of ER are the same in the four cases 1, 4, 5, and 6, and their indicators are much smaller than those of the system without the presence of ER.

Figure 15 is the radar chart of the power quality index; the system using ER uses warm thread and the system without ER uses cool thread. In this picture, the lines of cool colors are seen in the outer circle and the lines of warm colors are seen in the inner circle. Figure 15 thus indicates that the use of ER has greatly improved the power quality index.

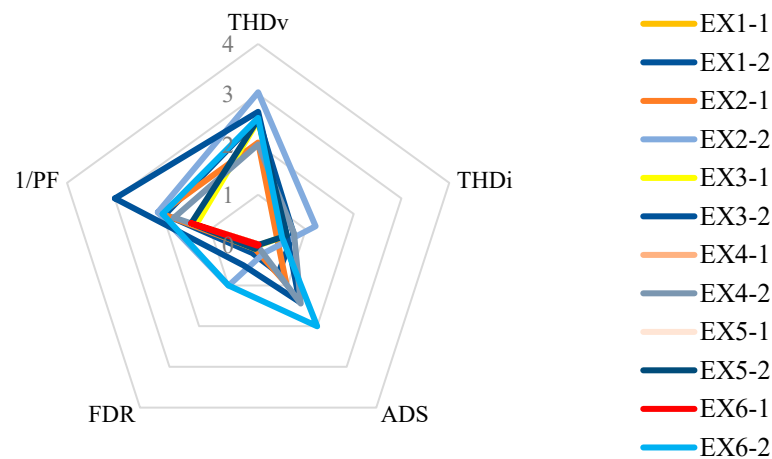


Figure 15. Power quality radar chart.

Under several specific experimental conditions, the ER does not interact with the grid at all. All the energy has been consumed under the regulation of ER, and does not need to be transmitted to the grid through the grid-connected port. If there is no energy interaction, there will be no power quality problems.

In cases 2 and 3, the ER acts as a primary distribution of energy structure, first routing the energy internally before interacting with the distribution grid. The resulting “energy gap” is filled by the distribution grid. Therefore, in this case, the energy that interacted with the distribution grid is the “missing energy”, which is obviously smaller than the total energy, and the energy interaction type changes from two ($P_{pv} + P_{load}$) to one ($P_{pv} - P_{load}$), which improves the power quality.

5. Conclusions

In this paper, a five-port ER model is first established, and the corresponding control strategy and energy scheduling method are designed for this topology. The feasibility of the topology and the control strategy is verified by simulation experiments.

In the second step, an IEEE13 node active distribution grid model is built. It connects PV, energy storage, and AC/DC loads to this system. In the traditional active distribution network model, all structures are connected to PCC nodes. For this structure, a power quality assessment system based on hierarchical analysis is designed to evaluate the strengths and weaknesses of power quality. When the load fluctuates, the power quality will fluctuate.

When we connect ER to the active distribution network, ER acts as a transit station and can well coordinate the flow of energy while regulating the power quality. We verified two points through our quantitative experiments. First, we verified the feasibility of the five-port ER topology and the control strategy, and second, we verified how ER access can enhance the power system.

Author Contributions: Conceptualization, X.C., Y.L., D.Y., T.J. and M.A.M.; methodology, X.C., Y.L., D.Y., T.J. and M.A.M.; validation, X.C., Y.L., D.Y., T.J. and M.A.M.; formal analysis, X.C., Y.L., D.Y., T.J. and M.A.M.; investigation, X.C., Y.L., D.Y., T.J. and M.A.M.; writing—original draft preparation, X.C., Y.L., D.Y., T.J. and M.A.M.; writing—review and editing, X.C., Y.L., D.Y., T.J. and M.A.M.; supervision, T.J. and M.A.M. All authors have read and agreed to the published version of the manuscript.

Funding: This work was supported by the Chinese National Natural Science Foundation (grant number 51977039) and the central government guiding local science and technology development project under grant number 2021L3005.

Institutional Review Board Statement: Not applicable.

Informed Consent Statement: Not applicable.

Data Availability Statement: Not applicable.

Conflicts of Interest: The authors declare no conflict of interest.

Nomenclature

ER	Energy router
PV	Photovoltaic
EI	Energy Internet
CB	Common bus
U_{cb}	Common bus voltage
I_d	Three-phase grid current active component
I_q	Three-phase grid current reactive component
I_d^*	Three-phase grid current active component reference value
I_q^*	Three-phase grid current reactive component reference value
U_d	Three-phase grid voltage active component
U_q	Three-phase grid voltage reactive component
U_d^*	Three-phase grid voltage active component reference value
U_q^*	Three-phase grid voltage reactive component reference value
MPC	Model pretend control
$i_l(k)$	Energy storage port k moment inductor current
$i_l(k + 1)$	Energy storage port $k + 1$ moment inductor current (Predicted value)
T_s	System sampling period
P_{load}	Load power, including the sum of DC and AC load power
P_{pv}	Photovoltaic power
SOC	Battery state of charge
AHP	Analytic hierarchy process
CI	Consistency index of AHP
CR	Consistency ratio of AHP
Nf	Dimension of the judgment matrix
RI	Average random consistency index related to the dimension of the judgment matrix.
PQI	Power quality index
PCC	Common coupling point
W_{pcc}	Average reliable weight vector of PCC bus

References

1. Hebal, S.; Harous, S.; Mechta, D. Energy Routing Challenges and Protocols in Energy Internet: A Survey. *J. Electr. Eng. Technol.* **2021**, *16*, 3197–3212. [[CrossRef](#)]
2. Abdella, J.; Shuaib, K. Peer to Peer Distributed Energy Trading in Smart Grids: A Survey. *Energies* **2018**, *11*, 1560. [[CrossRef](#)]
3. Chen, D.; Hu, X.; Li, Y.; Abbas, Z.; Wang, R.; Li, D. Nodal conservation principle of potential energy flow analysis for energy flow calculation in energy internet. *Energy* **2023**, *263*, 125562. [[CrossRef](#)]
4. Feng, C.; Liao, X. An overview of “Energy + Internet” in China. *J. Clean. Prod.* **2020**, *258*, 120630. [[CrossRef](#)]
5. Jiao, W.; Chen, J.; Wu, Q.; Li, C.; Zhou, B.; Huang, S. Distributed Coordinated Voltage Control for Distribution Networks With DG and OLTC Based on MPC and Gradient Projection. *IEEE Trans. Power Syst.* **2022**, *37*, 680–690. [[CrossRef](#)]
6. Liu, Y.; Jin, T.; Mohamed, M.A.; Wang, Q. A Novel Three-Step Classification Approach Based on Time-Dependent Spectral Features for Complex Power Quality Disturbances. *IEEE Trans. Instrum. Meas.* **2021**, *70*, 1–14. [[CrossRef](#)]
7. Syed, I.; Khadkikar, V.; Zeineldin, H.H. Loss Reduction in Radial Distribution Networks Using a Solid-State Transformer. *IEEE Trans. Ind. Appl.* **2018**, *54*, 5474–5482. [[CrossRef](#)]
8. Liu, Y.; Yuan, D.; Gong, Z.; Jin, T.; Mohamed, M.A. Adaptive spectral trend based optimized EWT for monitoring the parameters of multiple power quality disturbances. *Int. J. Electr. Power Energy Syst.* **2023**, *146*, 108797. [[CrossRef](#)]
9. Cardiel-Alvarez, M.A.; Rodriguez-Amenedo, J.L.; Arnaltes, S.; Montilla-DJesus, M.E. Modeling and Control of LCC Rectifiers for Offshore Wind Farms Connected by HVDC Links. *IEEE Trans. Energy Convers.* **2017**, *32*, 1284–1296. [[CrossRef](#)]
10. Mahela, O.P.; Shaik, A.G. Power quality improvement in distribution network using DSTATCOM with battery energy storage system. *Int. J. Electr. Power Energy Syst.* **2016**, *83*, 229–240. [[CrossRef](#)]
11. Du, W.; Schneider, K.P.; Wiegand, G.P.; Tuffner, F.K.; Xie, J.; Dent, O.L. A Supplemental Control for Dynamic Voltage Restorers to Improve the Primary Frequency Response of Microgrids. *IEEE Trans. Smart Grid* **2022**, *1*. [[CrossRef](#)]
12. Jia, W.; Guo, Q.; Tu, C.; Jiang, F.; Wang, L.; Hou, Y. Improved Single-phase UPQC with Integrating Auxiliary Capacitor for Power Rating Reduction. *IEEE Trans. Ind. Electron.* **2022**, 1–11. [[CrossRef](#)]
13. Prakash Mahela, O.; Gafoor Shaik, A. Topological aspects of power quality improvement techniques: A comprehensive overview. *Renew. Sustain. Energy Rev.* **2016**, *58*, 1129–1142. [[CrossRef](#)]

14. Chen, R.; Yang, Y.; Jin, T. A hierarchical coordinated control strategy based on multi-port ER of urban rail transit. *Prot. Control Mod. Power Syst.* **2022**, *7*, 2205. [[CrossRef](#)]
15. Zhu, L.; Rong, X.; Zhao, J.; Zhang, H.; Zhang, H.; Jia, C.; Ma, G. Topology optimization of AC/DC hybrid distribution network with ER based on power flow calculation. *Energy Rep.* **2022**, *8*, 1622–1638. [[CrossRef](#)]
16. Abdallah, W.J.; Hashmi, K.; Faiz, M.T.; Flah, A.; Channumsin, S.; Mohamed, M.A.; Ustinov, D.A. A Novel Control Method for Active Power Sharing in Renewable-Energy-Based Micro Distribution Networks. *Sustainability* **2023**, *15*, 1579. [[CrossRef](#)]
17. Li, P.; Sheng, W.; Duan, Q.; Li, Z.; Zhu, C.; Zhang, X. A Lyapunov Optimization-Based Energy Management Strategy for Energy Hub With ER. *IEEE Trans. Smart Grid* **2020**, *11*, 4860–4870. [[CrossRef](#)]
18. Tu, C.; Xiao, F.; Lan, Z.; Guo, Q.; Shuai, Z. Analysis and Control of a Novel Modular-Based ER for DC Microgrid Cluster. *IEEE J. Emerg. Sel. Top. Power Electron.* **2019**, *7*, 331–342. [[CrossRef](#)]
19. Jordehi, A.R.; Tabar, V.S.; Mansouri, S.A.; Sheidaei, F.; Ahmarinejad, A.; Pirouzi, S. Two-stage stochastic programming for scheduling microgrids with high wind penetration including fast demand response providers and fast-start generators. *Sustain. Energy Grids Netw.* **2022**, *31*, 100694. [[CrossRef](#)]
20. Nasir, M.; Jordehi, A.R.; Tostado-Véliz, M.; Tabar, V.S.; Mansouri, S.A.; Jurado, F. Operation of energy hubs with storage systems, solar, wind and biomass units connected to demand response aggregators. *Sustain. Cities Soc.* **2022**, *83*, 103974. [[CrossRef](#)]
21. Khalid, H.M.; Muyeen, S.M.; Kamwa, I. An improved decentralized finite-time approach for excitation control of multi-area power systems. *Sustain. Energy Grids Netw.* **2022**, *31*, 100692. [[CrossRef](#)]
22. Mahela, O.P.; Khan, B.; Alhelou, H.H.; Siano, P. Power Quality Assessment and Event Detection in Distribution Network With Wind Energy Penetration Using Stockwell Transform and Fuzzy Clustering. *IEEE Trans. Ind. Inf.* **2020**, *16*, 6922–6932. [[CrossRef](#)]
23. Xu, Y.; Fan, S.; Xie, S.; Lu, M. Power quality detection and classification in high permeability active distribution network based on IEWT-MFDE. *CSEE JPES* **2022**, *8*, 1646–1658.
24. Elbasuony, G.S.; Abdel Aleem, S.H.E.; Ibrahim, A.M.; Sharaf, A.M. A unified index for power quality evaluation in distributed generation systems. *Energy* **2018**, *149*, 607–622. [[CrossRef](#)]
25. Xu, Y.; Gao, Y.; Li, Z.; Lu, M. Detection and classification of power quality disturbances in distribution networks based on VMD and DFA. *CSEE JPES* **2020**, *6*, 122–130.
26. Ahmarinejad, A. A Multi-objective Optimization Framework for Dynamic Planning of Energy Hub Considering Integrated Demand Response Program. *Sustain. Cities Soc.* **2021**, *74*, 103136. [[CrossRef](#)]
27. Mansouri, S.A.; Nematbakhsh, E.; Ahmarinejad, A.; Jordehi, A.R.; Javadi, M.S.; Marzband, M. A hierarchical scheduling framework for resilience enhancement of decentralized renewable-based microgrids considering proactive actions and mobile units. *Renew. Sustain. Energy Rev.* **2022**, *168*, 112854. [[CrossRef](#)]
28. Nascimento, R.; Ramos, F.; Pinheiro, A.; Junior, W.D.A.S.; Arcanjo, A.M.; Filho, R.F.D.; Mohamed, M.A.; Marinho, M.H. Case Study of Backup Application with Energy Storage in Microgrids. *Energies* **2022**, *15*, 9514. [[CrossRef](#)]
29. Alsokhry, F.; Siano, P.; Annuk, A.; Mohamed, M.A. A Novel Time-of-Use Pricing Based Energy Management System for Smart Home Appliances: Cost-Effective Method. *Sustainability* **2022**, *14*, 14556. [[CrossRef](#)]
30. Ali, A.I.M.; Alaas, Z.M.; Sayed, M.A.; Almalaq, A.; Farah, A.; Mohamed, M.A. An Efficient MPPT Technique-Based Single-Stage Incremental Conductance for Integrated PV Systems Considering Flyback Central-Type PV Inverter. *Sustainability* **2022**, *14*, 12105. [[CrossRef](#)]
31. Chen, W.; Liu, B.; Nazir, M.S.; Abdalla, A.N.; Mohamed, M.A.; Ding, Z.; Bhutta, M.S.; Gul, M. An energy storage assessment: Using frequency modulation approach to capture optimal coordination. *Sustainability* **2022**, *14*, 8510. [[CrossRef](#)]
32. Mohamed, M.A.; Diab, A.A.Z.; Rezk, H.; Jin, T. A novel adaptive model predictive controller for load frequency control of power systems integrated with DFIG wind turbines. *Neural Comput. Appl.* **2020**, *32*, 7171–7181. [[CrossRef](#)]
33. Jin, T.; Guo, J.; Mohamed, M.A.; Wang, M. A novel model predictive control via optimized vector selection method for common-mode voltage reduction of three-phase inverters. *IEEE Access* **2019**, *7*, 95351–95363. [[CrossRef](#)]

Disclaimer/Publisher’s Note: The statements, opinions and data contained in all publications are solely those of the individual author(s) and contributor(s) and not of MDPI and/or the editor(s). MDPI and/or the editor(s) disclaim responsibility for any injury to people or property resulting from any ideas, methods, instructions or products referred to in the content.